Journal of Applied Analysis and Computation
Volume 17, Number 3, June 2027, 2034–2051
Website:http://www.jaac-online.com
DOI:10.11948/20250150

ENTRY-EXIT TRANSITION INDUCED MIXED-MODE OSCILLATIONS IN A THREE-TIME SCALE NEURAL MODEL

Yaru Liu[1], Rui Qi[1,†] and Shenquan Liu[2]

Abstract This paper investigates the entry-exit transition induced mixed-mode states (i.e., alternating subthreshold oscillations and large-amplitude spikes) in a three-time-scale FitzHugh-Nagumo-Rinzel neural model. Among these, mixed-mode oscillations (MMOs) represent a characteristic rhythm in neural models, yet elucidating their underlying mechanisms remains challenging due to the interplay of multi-time scale dynamics. This study specifically investigates the inherent relationship between MMOs and degenerate multi-time scale dynamics, where the normal hyperbolicity of the critical manifold is lost at fold point when normal hyperbolicity breaks up: A configuration that fundamentally complicates the analysis of their interaction. To address this complexity, we employ a geometric singular perturbation theory (GSPT)-based blow-up strategy for rigorous three-time-scale analysis. Through rigorous theoretical analysis, we establish a critical connection between the system's return map mechanism and MMOs generation. By constructing well-defined coordinate transformations, we demonstrate that asymptotic transitions in the desingularized system govern the emergence of MMOs, providing a mathematical proof for this dynamical transition. Notably, our numerical simulations reveal a 1^{25}-type MMOs pattern through systematic parameter variation, corroborating theoretical predictions. The proposed methodology establishes a framework for analyzing oscillation mechanisms in non-hyperbolic systems with multiple time scales, offering insights applicable to both computational neuroscience and nonlinear dynamics research.

Keywords Neuron model, MMOs, GSPT, multi-time scale dynamics, blow-up.

MSC(2010) 37F45, 39A21, 70G60, 70K50, 74H60.

1. Introduction

Neuron models, which are fundamental to neuroscience, are typically based on the dynamics of neural cells. Most classically, Hodgkin-Huxley (HH) model, which was awarded a Nobel prize, has been extensively studied and serves as a cornerstone in the field. Building on this foundation, a variant of the FitzHugh-Nagumo-Rinzel (FNR) model has emerged as a modified and analytically tractable simplification of the HH model [17,44], originally developed by FitzHugh R. [12], Nagumo J. [38], and later refined by Rinzel J. [40]. In this study, we focus on an extended version of the FNR model [53], aiming to develop an asymptotic expression for its return map, which provides critical insights into the dynamical behavior of neuronal systems [16].

In addition, neuron models are renowned for their rich dynamical properties, which manifest in a variety of discharge patterns, including bursting and oscillations. Specifically, mixed-mode oscillations (MMOs) represent a particularly intriguing class of behaviors, initially identified in

[†]The corresponding author.
[1]Department of Mathematics, Jinan University, Guangzhou 510632, China
[2]School of Mathematics, South China University of Technology, Guangzhou 510640, China
Email: yaruliu879@jnu.edu.cn(Y. Liu), 2018987259@qq.com(R. Qi), mashqliu@scut.edu.cn(S. Liu)

the context of Belousov-Zhabotinsky chemical reactions [15,45,54]. Since their discovery, MMOs have been the subject of extensive theoretical and numerical investigations, not only in neuronal and biological models but also in a wide range of other dynamical systems [13,19,32,35,36,42,43,47]. From a mathematical view, elucidating the mechanisms underlying canard-induced MMOs is a particularly critical research area [22, 23, 41]. Furthermore, MMOs are typically observed in multi-timescale dynamical systems, such as neuron models, which can be effectively analyzed by decomposing them into subsystems [2, 4, 25, 33, 34, 46, 53].

In the context of multi-timescale dynamical systems, singular perturbation theories have emerged as a foundational framework for analyzing the existence and bifurcation of canards in R^3 [1, 52]. These theories offer profound insights into singular Hopf bifurcations and the mechanisms driving relaxation oscillations in systems characterized by two slow variables [3, 14, 21, 23, 24, 37, 47]. However, a critical challenge arises near fold points, where the normal hyperbolicity of the system can be disrupted due to its singularities exist. To address this, the blow-up method, pioneered by Dumortier et al. [8], has been established as an effective technique for resolving such singularities and restoring analytical tractability [1, 18, 20]. On a macro level, Zhang et al. uses artificial neural networks to learn spiking neural networks and discover and study neural oscillations [9, 39, 49, 55]. In recent years, research on the mixed-mode oscillation mechanism has become increasingly profound [26, 31, 48]. In this work, we focus on unraveling the entry-exit mechanism of the return map in a neuron model, providing a comprehensive description of the resulting MMOs. Singularly perturbed systems are widely studied in control engineering due to their practical significance [7, 27–29, 50, 51]. Meanwhile, intelligent approaches, such as deep reinforcement learning [6,30] and neural network prediction models [5, 10, 11, 56], are increasingly adopted for complex engineering tasks.

This paper is organized as follows. Section 2 introduces the proposed model and its theoretical framework. In Section 3, we provide a comprehensive analysis of the return map mechanism for elucidating its dynamical properties. Section 4 presents numerical simulations to validate the theoretical findings and discusses the key conclusions of the study. Finally, Section 5 summarizes the main results and their implications. For completeness, the detailed proofs and technical derivations related to Section 3 are included in the appendix.

2. Model

We first consider an extended formulation of the classical FitzHugh-Nagumo equations, with a particular focus on their dynamical properties in the neighborhood of an arbitrary generic point $P = (v_0, z_0, w_0)$. The governing equations are presented as follows [12, 13, 20, 35–38, 42, 47, 53]:

$$\begin{cases} \varepsilon v' = -z + v^2 - \dfrac{1}{3}v^3, & (2.1a) \\ z' = 2v - 2 + a - c + (d-b)w - b(z+z_0) + dw_0, & (2.1b) \\ w' = \varepsilon(-v + 1 + c - d(w+w_0)), & (2.1c) \end{cases}$$

let $a = -0.992370, b = 0.002, c = -30, d = 60, z_0 = 0.3, w_0 = 0.9$, while perturbed parameter $0 < \varepsilon \ll 1$. Meanwhile, the derivative v, z and w are all of time τ. To avoid redundancy, this notation will not be repeated in the next analysis.

$$\begin{cases} \varepsilon v' = -z + v^2 - \dfrac{1}{3}v^3, & (2.2a) \\ z' = 2v + 59.998w - 0.002z + 81.00703, & (2.2b) \\ w' = \varepsilon(-v - 60w - 83). & (2.2c) \end{cases}$$

The coefficient 59.998 is obtained from the parameters in Eq. (2.1b) as $d-b=59.998$. By applying geometric singular perturbation theory (GSPT) and employing the time-scale transformation $t=\frac{\tau}{\varepsilon}$, as established by Krupa et al. [20], the system defined by (2.2a)-(2.2c) can be constrained to the following form:

$$\begin{cases} v' = -z + v^2 - \dfrac{1}{3}v^3, & \text{(2.3a)} \\ z' = \varepsilon(2v + 59.998w - 0.002z + 81.00703), & \text{(2.3b)} \\ w' = \varepsilon^2(-v - 60w - 83). & \text{(2.3c)} \end{cases}$$

Our goal in this paper is to characterize the asymptotic return trajectories along the singular flow of system (2.2a)-(2.2c). As the system parameters vary, small-amplitude MMOs arise when singular canards traverse the explosion region near the origin on the (v,z,w)-plane for Eqs. (2.2a)-(2.2c). We further explore large-amplitude MMOs generated by the return map, which propagate canards along the fold line l^- after it has moved to the origin [2, 15, 25, 34, 45]. As for system (2.2a)-(2.2c), the paper systematically elucidates how MMOs yield through four key steps: Firstly, the flow dynamics are rigorously analyzed near the fold line l^-; hence, we provide a detailed mechanism governing the entry-exit transition within the fold region is established; finally, this the global return mechanism is comprehensively summarized. To facilitate this analysis, combining the fold line dynamics for Eqs. (2.2a)-(2.2c), we now introduce the following rescaled variables $v=\sqrt{\varepsilon}\bar{v}, \bar{t}=\sqrt{\varepsilon}t, z=\varepsilon\bar{z}, w=\sqrt{\varepsilon}\bar{w}$ for (2.2a)-(2.2c), then obtain

$$\begin{cases} \bar{v}' = -\bar{z} + \bar{v}^2 - \dfrac{1}{3}\sqrt{\varepsilon}\bar{v}^3, & \text{(2.4a)} \\ \bar{z}' = 2\bar{v} + 59.998\bar{w} - 0.002\sqrt{\varepsilon}\bar{z} + 81.00703, & \text{(2.4b)} \\ \bar{w}' = \varepsilon(\mu - \sqrt{\varepsilon}(d\bar{w} + \bar{v})), & \text{(2.4c)} \end{cases}$$

where $\mu=-83$, which is obtained from Eq. (2.3c). In this context, the prime symbol represents differentiation with respect to the rescaled time $\bar{t}$; for notational simplicity, we use t instead. When $\varepsilon=0$, the system described by Eqs. (2.4a)-(2.4c) simplifies to the following form:

$$\begin{cases} \bar{v}' = -\bar{z} + \bar{v}^2, & \text{(2.5a)} \\ \bar{z}' = 2\bar{v} + 59.998\bar{w} + \chi, & \text{(2.5b)} \end{cases}$$

where $\chi = a - c - bz_0 + dw_0 - 2 = 81.00703$. Thus, for the prototypical system, canard explosion occurs at $\chi=0$. Particularly, (2.5a)-(2.5b) is integrable for $\bar{w}=0$, then the system exhibits the following properties

$$\begin{cases} \bar{v}' = -\bar{z} + \bar{v}^2, & \text{(2.6a)} \\ \bar{z}' = 2\bar{v}. & \text{(2.6b)} \end{cases}$$

The system described by Eqs. (2.5a)-(2.5b) is integrable, with the constant of motion given by $H(\bar{v},\bar{z}) = e^{-\bar{z}}(\bar{v}^2 - \bar{z} - 1)$. We now turn to Eqs. (2.6a)-(2.6b), which admit a family of periodic orbits defined by the level curves $H(\bar{v},\bar{z})=h$, with h real; the singular solution corresponding to $h=0$, which is given by $\bar{\gamma}_0^0(t) = (\bar{v}_0^0, \bar{z}_0^0)(t) = (\frac{1}{2}t, \frac{1}{4}t^2 - 1)$, which represents an invariant parabola. The geometry of this parabola curves in Eqs. (2.6a)-(2.6b) are illustrated in Figure 1(b), (c) and (d). Notably, the level curves of H that are divided as for $h>0$ (generate periodic solutions) from the open ones, which are characterised by $h<0$ (correspond to trajectories that leave the fold region). Furthermore, for any $h<0$, we derive $\bar{z}^h$ in $\bar{\Delta}_-$, where $\bar{\Delta}_-$ denotes the

half-plane $\bar{\Delta} \cap \{\bar{z} < 0\}$. For any fold point $(0, \bar{z}^h, \bar{w}) \in \bar{\Delta}_-$, $\bar{\gamma}_\varepsilon^h$ represents the solution of Eqs. (2.4a)-(2.4c). Assuming $\bar{\gamma}_\varepsilon^h(-T^h(\bar{w})) = (0, \bar{z}^h, \bar{w})$ (T^h represents the required transition time under their respective return map when $H(\bar{v}, \bar{z}) = h$), the solution $\bar{\gamma}_\varepsilon^h(T^h(\bar{w})$ first returns to $\bar{\Delta}_-$, as depicted in Figure 1(c). Additionally, we examine the case $\bar{w} = 0$, for which $T^h = T^h(0)$. Conversely, for a fixed $h > 0$, $\bar{\gamma}_h^0$ corresponds to the periodic solution of Eqs. (2.6a)-(2.6b). Importantly, ξ_h and ζ_h denote the two intersection points of $\bar{\gamma}_0^h$ with $\bar{\Delta}$, corresponding to their $\bar{z}$-coordinates, respectively [2, 15, 25, 34, 45]; see Figure 1(d).

Table 1. Summary of specialized mathematical symbols and detailed descriptions in paper. (The detailed names can be referred to Refs. [20, 21, 33, 34].)

Symbols	Introduction of section for Eqs. (2.1)
Δ	where $v = 0$, with $\|z\|$ and $\|w\|$ bounded
$\bar{\Delta}$	where $\bar{v} = 0$, with $\|\bar{z}\|$ and $\|\bar{w}\|$ bounded
$\bar{\Delta}_-$	the portion of $\bar{\Delta}$ where $\bar{z} < 0$ ($\bar{\Delta}_- \subset \bar{\Delta}$)
$\bar{\Delta}_+$	$\bar{\Delta}_+ = \bar{\Delta} \setminus \bar{\Delta}_-$
$\bar{\Delta}_{\text{in}}$	$\bar{\Delta}_{\text{in}} = \{(\bar{v}, \bar{z}, \bar{w}) \| \bar{v} = -\alpha, 0 < \alpha < \rho\}$
$\bar{\Delta}_{\text{out}}$	$\bar{\Delta}_{\text{out}} = \bar{\Pi}^{\text{out}}(\bar{\Delta}_-)$
Σ^{in}	where $v = -\rho$, with $\|z\|$ and $\|w\|$ bounded
Σ^{out}	where $v = \delta$, with $\|z\|$ and $\|w\|$ bounded
Π	$\bar{\Delta}_- \to \bar{\Delta}_-$
$\bar{\Pi}$	$\bar{\Delta}_- \to \bar{\Delta}_-$
Π^{in}	$\bar{\Delta}^{\text{in}} \to \bar{\Delta}_-$
$\bar{\Pi}^{\text{in}}$	$\Sigma^{\text{in}} \to \bar{\Delta}_-$
Π_{ret}	$\Sigma^{\text{out}} \to \Sigma^{\text{in}}$

Lemma 2.1. *There exists $T^h = (-\text{lnh})^{\frac{1}{2}} + \mathcal{O}(1)$ for Eqs. (2.6a)-(2.6b) where $\zeta^h = -\text{lnh} + \mathcal{O}(1)$ and $\xi^h = -1 + \mathcal{O}(h)$.*

Proof. From the preceding analysis, and given the relation $h(\bar{v}, \bar{z})e^{\bar{z}} = \bar{v}^2 - \bar{z} - 1$, we obtain $\bar{v} = \sqrt{\bar{z}}\sqrt{1 + \frac{1}{\bar{z}} + h(\bar{v}, \bar{z})\frac{e^{\bar{z}}}{\bar{z}}}$. By leveraging the identity $\bar{v} = \frac{\bar{z}'}{2} = \frac{1}{2} \cdot \frac{d\bar{z}}{dt}$ for $\bar{w} = 0$, we integrate the above equation to arrive at the following result:

$$\begin{aligned} T^h = &\sqrt{\bar{z}}(1 + \frac{1}{\bar{z}} - h(\bar{v}, \bar{z})\frac{e^{\bar{z}}}{\bar{z}})^{-\frac{1}{2}} \Big|_{\xi^h}^{\zeta^h} \\ &+ \frac{1}{2}\int_{\xi^h}^{\zeta^h} \sqrt{\bar{z}}(1 + \frac{1}{\bar{z}} + h(\bar{v}, \bar{z})\frac{e^{\bar{z}}}{\bar{z}})^{-\frac{3}{2}}(-\frac{1}{\bar{z}^2} + h(\bar{v}, \bar{z})\frac{e^{\bar{z}}}{z^2}(\bar{z} - 1))d\bar{z}. \end{aligned} \tag{2.7}$$

From Lemma A.1 in Ref. [20], for $\bar{v} = 0$ within the region $\bar{\Delta}_-$, the relation $\bar{z} + 1 = he^{\bar{z}}$ holds for $\bar{z}$ sufficiently large and constant. This yields the asymptotic expressions $\zeta^h = -\text{lnh} + \mathcal{O}(1)$ and $\xi^h = -1 + \mathcal{O}(h)$ [2, 25, 33, 34]. Furthermore, the boundaries of ζ^h and ξ^h determine the leading-order term in Eq. (2.7). Upon expanding the second term, we observe that its corresponding integral contributes only terms of order $\mathcal{O}(1)$. Consequently, we establish that $T^h \sim \sqrt{\zeta^h} \sim (-\text{lnh})^{\frac{1}{2}}$, which completes the proof. □

In accordance with Lemma 2.1, we introduce the return map $\bar{\Pi}$ defined on $\bar{\Delta}_- \subset \bar{\Delta}$. The trajectories of (2.6a)-(2.6b) are uniquely parameterized by their unique h-value, while $\bar{z}^h$ is redefined in terms of the $\bar{z}$-values within $\bar{\Delta}_-$. Given that $\bar{\gamma}_\varepsilon^h(t)$ represents the solution of Eqs. (2.4a)-(2.4c) at the point $(0,\ \bar{z}^h,\bar{w})$, it follows that $\bar{\gamma}_\varepsilon^h(0)$ resides in $\bar{\Delta}_+ = \bar{\Delta} \setminus \bar{\Delta}_-$ under the chosen time parametrization, as depicted in Figure 1(c). Similarly, let $T_\pm^h(\bar{w})$ denote the times at which $\bar{\gamma}_\varepsilon^h(T_\pm^h(\bar{w})) \in \bar{\Delta}_-$, with $T_-^h(\bar{w}) < 0 < T_+^h(\bar{w})$, as illustrated in Figure 1(d). Here, we define $T^h(\bar{w}) := T_+^h(\bar{w}) - T_-^h(\bar{w})$. Finally, for $\bar{w} = 0$, there is $T^h := T_+^h(0) = -T_-^h(0)$ [2,25,33,34].

3. Return map mechanism analysis

This section presents the main theoretical results of the paper. The return map mechanism governing the entry-exit transition is analysed through three propositions. Based on the preceding analysis, we derive the asymptotic return map $\bar{\Pi} : \bar{\Delta}_- \to \bar{\Delta}_-$, as established in Propositions 3.1, 3.2, 3.3 [2,25,33,34].

Proposition 3.1. *Let $\varepsilon \in [0, \varepsilon_0]$, where $0 < \varepsilon_0 \ll 1$. Consider $(h, \bar{w}) \in \bar{\Delta}_-$ with $h > 0$ and $h = \mathcal{O}(\varepsilon^M)$, where $M > 0$. The transition map $\bar{\Pi}$ for Eq. (2.5) is*

$$\begin{aligned}(\hat{h}, \hat{\bar{w}}) &= \bar{\Pi}(h, \bar{w}) \\ &= (h + \sqrt{\varepsilon} d_{\sqrt{\varepsilon}}^h + \bar{w} d_{\bar{w}}^h + \mathcal{O}(2), \\ &\quad \bar{w}(1 - 30.001\varepsilon\sqrt{\varepsilon} T^h(\bar{w})) + \mathcal{O}(\varepsilon^2)),\end{aligned} \tag{3.1}$$

where $d_{\sqrt{\varepsilon}}^h = \int_{-T^h}^{T^h} \nabla H(\bar{\gamma}_0^h(t)) \cdot (-\frac{1}{3}\bar{v}_0^h(t)^3, 0)^T dt$, and $d_{\bar{w}}^h = \int_{-T^h}^{T^h} \nabla H(\bar{\gamma}_0^h(t)) \cdot (0, -1)^T dt$.

Proof. The detailed proof is provided in **Appendix 1**. □

Assumption 3.1. *For $0 < \varepsilon \ll 1$ in Eqs. (2.4a)-(2.4c), we assume $\bar{w} = O(\sqrt{\varepsilon})$ uniformly in $\bar{t}$, which implies $w = \sqrt{\varepsilon}\bar{w} = O(\varepsilon)$.*

By definition, $\bar{v}(-T^h) = \bar{v}(T^h) = 0$, and from Eq. (2.4b), it follows that $\frac{d\bar{z}}{dt} \sim -\bar{v}$. Based on Assumption 3.1, we conclude

$$\hat{w} \sim \bar{w} + 2\varepsilon(\mu T^h - g_1 \varepsilon \int_{\xi^h}^{\zeta^h} (\bar{v}(\bar{z}) - \frac{1}{3}\sqrt{\varepsilon}\bar{v}^2(\bar{z}))d\bar{z}, \tag{3.2}$$

where $\xi^h = \bar{z}(-T^h) \rightleftharpoons \bar{\gamma}_\varepsilon^h(-T^h)$ and $\zeta^h = \bar{z}(0) \rightleftharpoons \bar{\gamma}_\varepsilon^h(0)$ (The signal of "$\rightleftharpoons$" denotes correspondence to the $\bar{z}$-values in $\bar{\Delta}$) [2,25,33,34]. The condition $\bar{w} = \hat{w}$ requires $\mu T^h - g_1\varepsilon \int_{\xi^h}^{\zeta^h} (\bar{v}(\bar{z}) - \frac{1}{3}\sqrt{\varepsilon}\bar{v}^2(\bar{z}))d\bar{z} = 0$. This analysis identifies the canard boundaries $\bar{w}^c$ for Eqs. (2.4a)-(2.4c), expressed as: $\bar{w}^c = -\frac{d_{\sqrt{\varepsilon}}^0}{d_{\bar{w}}^0}\sqrt{\varepsilon} + \mathcal{O}(\varepsilon)$ where $d_{\sqrt{\varepsilon}}^0$ and $d_{\bar{w}}^0$ are derived from Eq. (3.1) in the limit $h \to 0$. To estimate Eq. (3.2), we observe $\frac{\partial H}{\partial \bar{v}} = -\bar{v}e^{-2\bar{z}}$, $\frac{\partial H}{\partial \bar{z}} = (\bar{v}^2 - \bar{z})e^{-2\bar{z}}$. Given $T^0 = \infty$, we obtain $d_{\sqrt{\varepsilon}}^0 = \frac{1}{16}\sqrt{2\pi}e, d_{\bar{w}}^0 = -\frac{1}{2}\sqrt{2\pi}e$, as demonstrated in Ref. [20]. Consequently, the value of $\bar{w}^c$ is $\bar{w}^c = \frac{1}{8}\sqrt{\varepsilon} + \mathcal{O}(\varepsilon) > 0$.

Our approach involves defining Π^{in} as the flow of Eqs. (2.2a)-(2.2c) in the fold region. We focus on a specific subset $\bar{\Delta}^{\text{in}} = \{(\bar{v}, \bar{z}, \bar{w}) \mid \bar{v} = -\alpha\}$ for Eqs. (2.4a)-(2.4c) where $0 < \alpha < \rho$. To proceed, we first establish Proposition 3.2, which characterizes the transition from Σ^{in} to $\bar{\Delta}_-$ [2,25,33,34].

Proposition 3.2. *Let* $(z^{in}, w^{in}) \in \Sigma^{in}$ *with* $\varepsilon > 0$. *The transition map* $\Pi^{in} : \Sigma^{in} \to \bar{\Delta}_-$ *satisfies* $(h^-, \bar{w}^-) := \Pi^{in}(z^{in}, w^{in}) = (\sqrt{\varepsilon} d^-_{\sqrt{\varepsilon}} + \frac{w^{in}}{\sqrt{\varepsilon}} d^-_{\bar{w}} + O(2), \frac{w^{in}}{\sqrt{\varepsilon}} + w^{in}\mu \ln\varepsilon + \mathcal{O}(\varepsilon^2)$, *where* $d^-_{\sqrt{\varepsilon}} = \int_{-\infty}^{0} \nabla H(\bar{\gamma}_0^0(t)) \cdot (-\frac{1}{3}\bar{v}_0^0(t)^3, 0)^T dt$, *and* $d^-_{\bar{w}} = \int_{-\infty}^{0} \nabla H(\bar{\gamma}_0^0(t)) \cdot (0, -1)^T dt$. *Here,* $\bar{\gamma}_0^0(t) = (\bar{v}_0^0, \bar{z}_0^0)(t)$ *is the solution of Eq. (3.1).*

Proof. For a detailed derivation of the proof, please refer to **Appendix 2**. □

Beyond the entry transition, we now investigate two distinct aspects of the exit transition. First, we analyze the flow transition for Eqs. (2.4a)-(2.4c), represented by $\bar{\Delta}^{\text{out}}$ where $T^{h,out}(\bar{w}) := -T_-^{-h}(\bar{w})$. Second, we study the transition $\bar{\Delta}^{\text{out}} \to \Sigma^{\text{out}}$ ($T^{h,out}$ represents the required transition $\bar{\Delta}^{\text{out}} \to \Sigma^{\text{out}}$ time under their respective return map when $H(\bar{v}, \bar{z}) = h$). Notably, when $h < 0$, trajectories may persist within the fold region. Especially, S_0 is a curve of equilibria for the layer problem obtained for $\varepsilon = 0$ in Eqs. (2.1) and is (normally) hyperbolic away from the two fold points where $z = v^2 - \frac{1}{3}v^3 = 0$; Finally, let $l^- = \{(0, 0, w)\}$ and $l^+ = \{(2, 0, w)\}$ denote the lower and upper fold lines for Eqs. (2.2), respectively, and note that $l^\pm$ are determined by imposing $z'(v) = 0$. Away from these fold lines, S_0 is normally hyperbolic; it consists of the two attracting sheets Eqs. (2.2) $S_0^{a-} = \{(v, z, w) | v < 0, z < 0\}$ and $S_0^{a+} = \{(v, z, w) | v > 2, z > \frac{4}{3}\}$, as well as of a repelling sheet which is given by $S_0^r = \{(v, z, w) | 0 < v < 2, 0 < z < \frac{4}{3}\}$. In this context, $\mathcal{C}_\varepsilon^a$ and $\mathcal{C}_\varepsilon^r$ denote the intersection components of S_ε^a and S_ε^r, respectively. As outlined in Refs. [20, 33], we explore the $\bar{z}$-coordinate of the curve $\mathcal{C}_\varepsilon^r$, which aligns parallel to the $\bar{w}$-plane in $\bar{\Delta}$ after reparameterizing $\bar{z}$ as a new variable $\tilde{z}$ [2, 25, 33, 34]:

Proposition 3.3. *Let* $(h, \bar{w}) \in \bar{\Delta}_-$ *with* $h = \mathcal{O}(\varepsilon^M) < 0$, *where* $M > 0$ *and* $\varepsilon \in [0, \varepsilon_0]$. *The map* $\Pi^{out} : \bar{\Delta}_- \to \Sigma^{out}$ *is defined as*

$$\begin{aligned}(z^{out}, w^{out}) :=& \Pi^{out}(h, \bar{w}) = (\varepsilon \tilde{z}^{out} + \mathcal{O}(\varepsilon \ln\varepsilon), \sqrt{\varepsilon}\bar{\mathrm{w}} \\ &- 83\varepsilon\sqrt{\varepsilon} T^{h,out}(\bar{w}) + \mathcal{O}(\varepsilon\sqrt{\varepsilon}),\end{aligned} \tag{3.3}$$

where $h^{out} = h + \sqrt{\varepsilon} d^{out}_{\sqrt{\varepsilon}} + \bar{w} d^{out}_{\bar{w}}$, *with* $d^{out}_{\sqrt{\varepsilon}} = -\int_0^{T^{h,out}(\bar{w})} \nabla H(\bar{\gamma}_0^0(t)) \cdot (-\frac{1}{3}\bar{v}_0^0(t)^3, 0)^T dt$, *and* $d^{out}_{\bar{w}} = -\int_0^{T^{h,out}(\bar{w})} \nabla H(\bar{\gamma}_0^0(t)) \cdot (0, -1)^T dt$.

Proof. A detailed derivation of the proof can be found in **Appendix 3**. □

We now summarize the global mechanism governed by the trajectories of Eqs. (2.2a)-(2.2c) through the map Π^{ret}: $\Sigma^{\text{out}} \to \Sigma^{\text{in}}$, which serves as the corresponding return map. Leveraging Fenichel's theorem and GSPT, Π^{out} offers a rigorous approximation for the total map Π. Building on Propositions 3.1, 3.2 and 3.3, we redefine map $\Pi : \bar{\Delta}_- \to \bar{\Delta}_-$ for Eqs. (2.2a)-(2.2c) in terms of Π^{ret}, $\bar{\Pi}$, Π^{in} and Π^{out}, leading to the following result [2, 25, 33, 34]

$$\Pi(h, \bar{w}) = \begin{cases} \bar{\Pi}(h, \bar{w}) & \text{if } h > 0 \\ \Pi^{\text{in}} \circ \Pi^{\text{ret}} \circ \Pi^{\text{out}}(h, \bar{w}) & \text{if } h < 0, \end{cases} \tag{3.4}$$

here Π represents the Poincaré map from Δ_- to itself, or equivalently, its 'blown-up' counterpart $\bar{\Delta}_-$ to itself.

4. Numerical analysis

Numerical simulations were performed in MATLAB using the fourth-order Runge-Kutta integration method. All graphical representations, including schematic diagrams, time series plots,

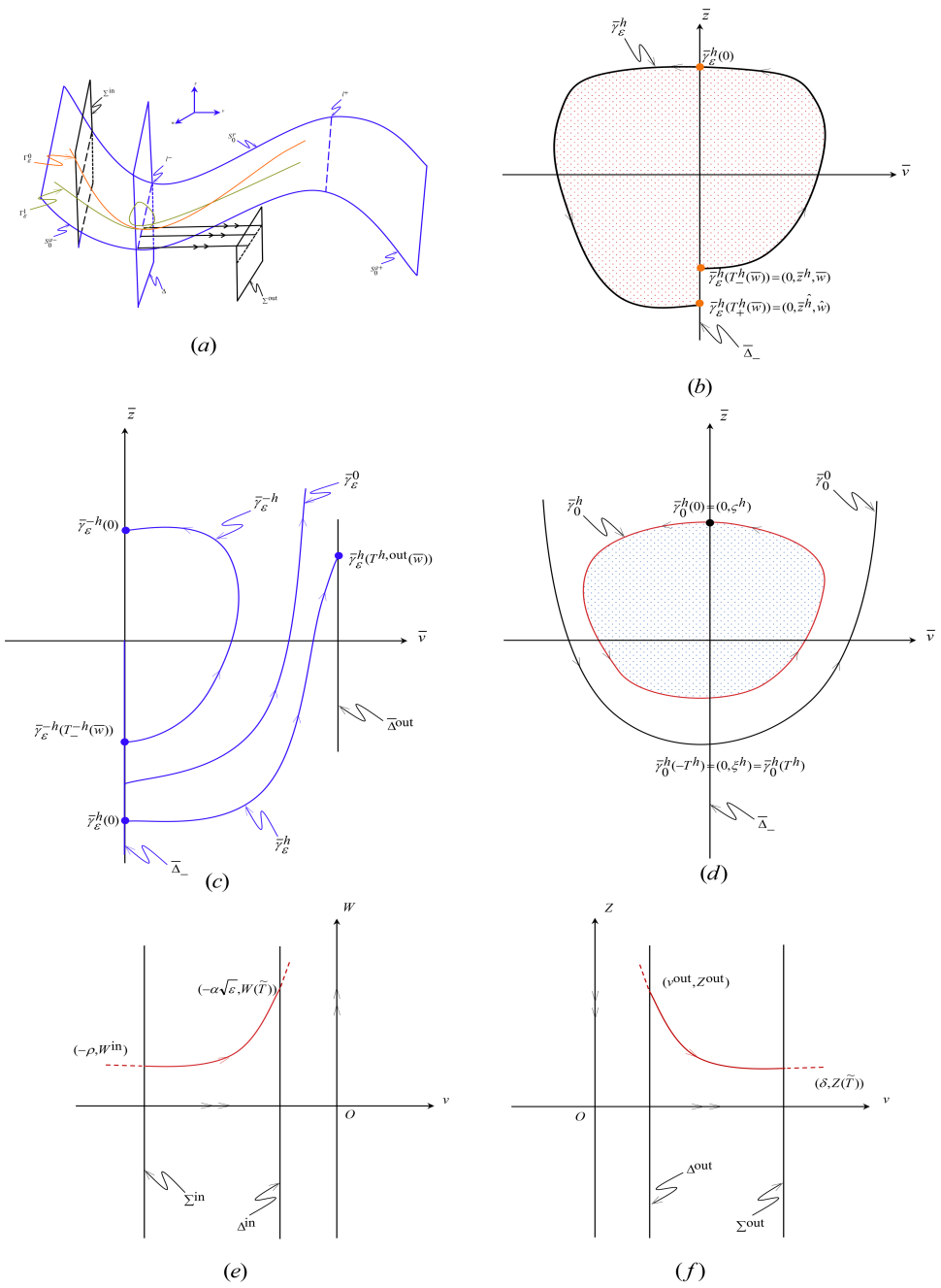

Figure 1. (a) Schematic diagram of Eq. (2.2), illustrating the critical manifold S_0 with its components $S_0^{a\pm}$ and S_0^r, fold lines $l^{\pm}$ and canards Γ_ε^0, Γ_ε^1. (b) Geometric representation of system (2.4a)-(2.4c) for $\varepsilon > 0$. (c) Plot of $T^{h,\text{out}}(\bar{w})$ for $h < 0$. (d) A typical solution of Eqs. (2.6a)-(2.6b). (e) Geometry structure of Eqs. (A5a)-(A5b). (f) Geometry structure of structure Eqs. (A3a)-(A3b) [20].

and phase portraits, were generated using Clickcharts 3.14, MATCONT, and OriginPro 2023b. Specifically, MATLAB was employed to simulate dynamical system outputs (e.g., time series data and phase-space trajectories), while OriginPro facilitated schematic modifications. Figure 1(a) illustrates the geometric structure of Eq. (2.2), comprising a critical manifold S_0 with two stable sheets $S_0^{a\pm}$ and one repulsive sheet S_0^r, fold lines $l^{\pm}$ (blue dotted), and canard tra-

jectories Γ_ε^0(orange) and Γ_ε^1 (green). Furthermore, two orthogonal black planes Σ^{in} and Σ^{out} intersect the S plane. In addition, Figure 1(b) demonstrates the perturbed geometry of system (2.4a)-(2.4c) under $\varepsilon > 0$. The threshold-dependent structure $T^{h,\text{out}}(\bar{w})$ for $h < 0$ is depicted in Figure 1(c), while Figure 1(d) presents a characteristic solution of Eqs. (2.6a)-(2.6b). Subsystems (A5a)-(A5b) and (A3a)-(A3b) are geometrically represented in Figure 1(e) and Figure 1(f), respectively. The above quoted formulas (A5a)-(A5b) and (A3a)-(A3b) with specific figures descriptions can be found in the **Appendixes 1-3**. In this work, Figure 2(a) displays 1^{25}-type MMOs through time series analysis, with Figure 2(b) showing the corresponding phase portrait in the (z, v)-plane. Specifically, the red dot denotes the Hopf point of the model (2.2a)-(2.2c) and the purple dashed line indicates the zero-isocline in Figure 2(b). Using MATCONT, we computed system parameters at Hopf bifurcation (denoted by H) and evaluated the first Lyapunov coefficient ($l_1(0)$) of the model (2.2a)-(2.2c). At Hopf point H, we reveal that the Jacobian matrix eigenvalues $\lambda_1 = -0.60433$, $\lambda_{2,3} = \pm 9.96413i$ for Eqs. (2.2a)-(2.2c). The negative first Lyapunov coefficient $l_1 = -38.2291$ at H point, confirms the stability of the Hopf equilibrium and identifies a supercritical Hopf bifurcation. In addition, we obtain the original signal using the "ode45" function and calculate the number of small peaks using the "findpeaks" function in Matlab, as shown in Figure 3. Based on the same system parameters as Figure 2, we select two detected period intervals to obtain Figure 3(a) (Early Detected Period: 200s-900s with 1416 small peaks) and Figure 3(b) (Post Detected Period: 845.8s-858.4s with 25 small peaks), respectively. Therefore, Figure 2(a) and Figure 3(b) displays 1^{25}-type MMOs for our model.

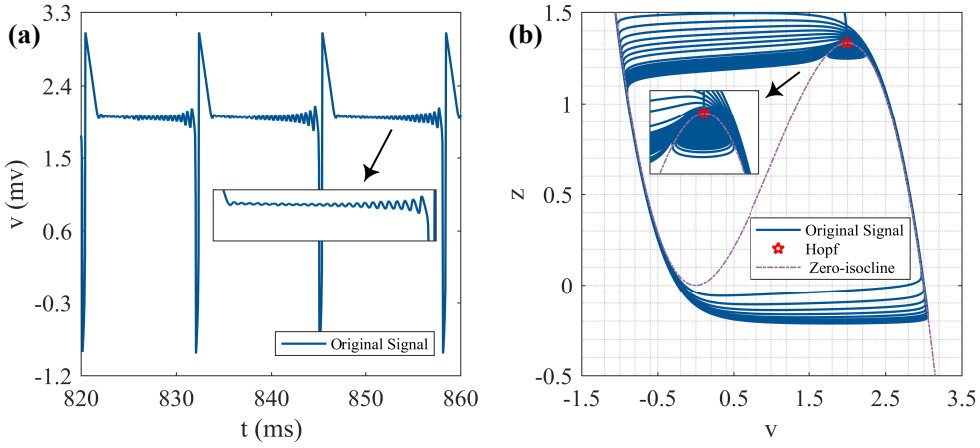

Figure 2. Dynamical characteristics of Eqs. (2.2a)-(2.2c) with parameters: $a = -0.992370, b = 0.002, c = -30, d = 60, \varepsilon = 0.01$. Initial conditions: $z_0 = 0.3, w_0 = 0.9$. Total simulation time: 2000 ms. (a) Time series exhibiting 1^{25}-type MMOs. (b) Corresponding phase portrait in the (z, v) plane.

5. Conclusions

This study establishes a theoretical framework elucidating the intrinsic connections between MMOs and multi-timescale dynamics in neural systems. To address the degeneracy arising from the loss of normal hyperbolicity, we implement the blow-up method for analyzing singular entry-exit transition dynamics. By employing GSPT and Fenichel's invariant theorem, we develop a three-scale analysis framework for the FitzHugh-Nagumo-Rinzel model under the asymptotic condition $\varepsilon \ll 1$. The principle mainly resides in the rigorous formulation of the return map mechanism through deterministic coordinate transformations for the FitzHugh-Nagumo-Rinzel

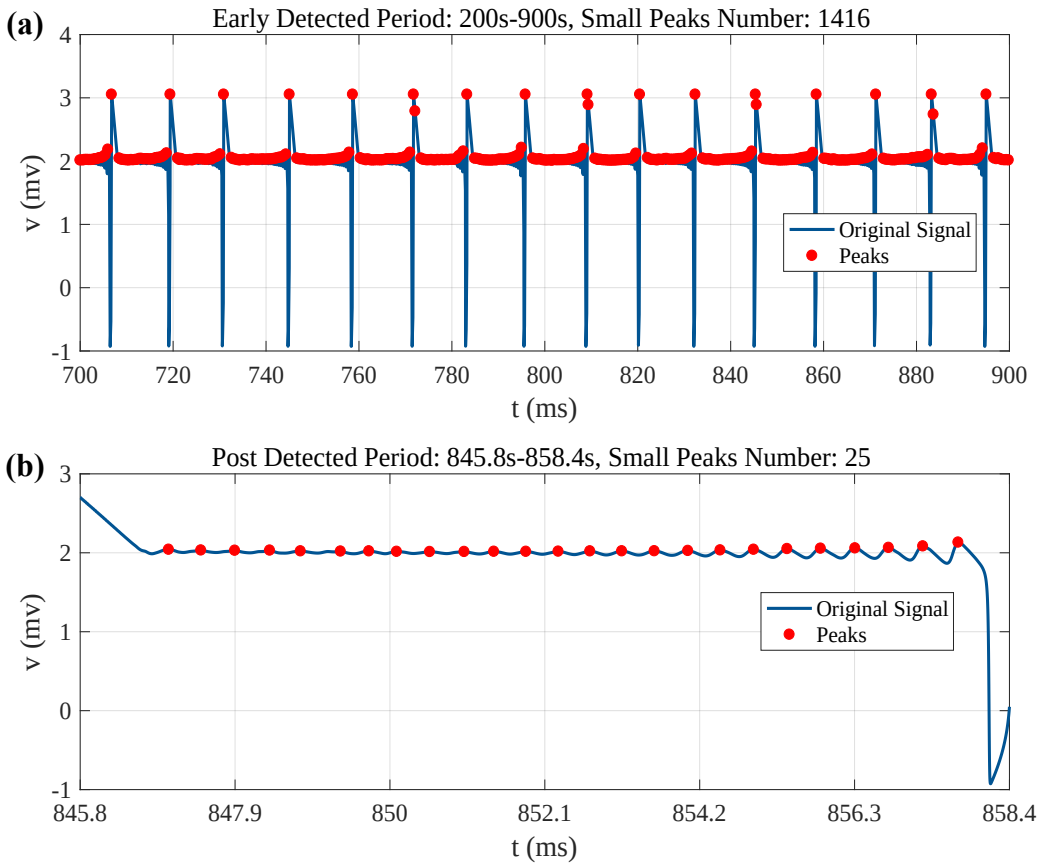

Figure 3. Original signal and peaks points of Eqs. (2.2a)-(2.2c) with parameters: $a = -0.992370, b = 0.002, c = -30, d = 60, \varepsilon = 0.01$. Initial conditions: $z_0 = 0.3, w_0 = 0.9$. (a) Early Detected Period: 200s-900s, Small Peaks Number: 1416. (b) Post Detected Period: 845.8s-858.4s, Small Peaks Number: 25.

model based on the methodology from Refs. [20,21]. Specifically, we derive an asymptotic expansion of the return map characterizing phase-space transitions from Σ^{in} into $\bar{\Delta}_-$ and subsequent transitions from $\bar{\Delta}_-$ to Σ_{out}. Complementing analytical proofs, numerical simulations provide dynamical verification of these theoretical propositions. Through systematic implementation of return map analysis, we demonstrate quantitative reconstruction of 1^{25}-type MMOs patterns as well as consistent agreement between schematic diagrams and time-series simulations. These findings apply a theoretical framework on FitzHugh-Nagumo-Rinzel model that bridges critical gaps in understanding scale interactions, while simultaneously benefit to promote the application of methodological approaches for MMOs analysis in neurodynamic systems.

Acknowledgments. This work was supported by the National Natural Science Foundation of China (Grant No. 12302069), the Guangzhou Municipal Science and Technology Bureau Project (Grant No. 2024A04J4029), the 2026 Youth Launch Project of Guangdong-Hong Kong-Macau Center for Applied Mathematics Grant No. 2026A1515060016, and the China Scholarship Council (CSC, No. 202406780055).

Data availability declarations. The authors declare that there is no potential commercial or financial conflict of interest. The data in the paper can be requested from the corresponding author.

Declarations conflict of interest. There are no conflicts of interest to declare.

A. Appendix 1

Proof of Proposition 3.1. Through systematic analysis of the governing Eqs. (2.4a)-(2.4c), we derive [2,25,33,34]

$$\begin{cases} \bar{v}' = -\bar{z} + \bar{v}^2 - \dfrac{1}{3}\sqrt{\varepsilon}\bar{v}^3 + \sqrt{\varepsilon}F(\bar{w},\sqrt{\varepsilon}) + \bar{w}G(\bar{w},\sqrt{\varepsilon}), & \text{(A1a)} \\ \bar{z}' = 2\bar{v} + 59.998\bar{w} - 0.002\sqrt{\varepsilon}\bar{z} + 81.00703 + \mathcal{O}(\varepsilon), & \text{(A1b)} \\ \bar{w}' = \varepsilon(\mu - \sqrt{\varepsilon}(d\bar{w} + \bar{v}) + \mathcal{O}(\varepsilon)), & \text{(A1c)} \end{cases}$$

where $\mu = -83$. To establish the main assertion for $\hat{h}$, defined as the image of the image of h under the projection operator $\bar{\Pi}$, we proceed as follows. By differentiating the Hamiltonian along the perturbed trajectory $\bar{\gamma}_\varepsilon^h(t)$, we obtain $\frac{d}{dt}H(\bar{\gamma}_\varepsilon^h(t)) = \nabla H(\bar{\gamma}_\varepsilon^h(t)) \cdot (\bar{v}', \bar{z}')^T \mid_{\bar{\gamma}_\varepsilon^h(t)}$. Given the boundary conditions $\hat{h} = H(0, \bar{z}^{\hat{h}})$ and $h = H(0, \bar{z}^h)$, we can derive

$$\begin{aligned} \hat{h} - h = &\int_{T_-^h(\bar{w})}^{T_+^h(\bar{w})} \nabla H(\bar{\gamma}_0^h(t)) \cdot (f_3\bar{v}_0^h(t)^3 + F(0,0), 0)^T dt\sqrt{\varepsilon} \\ &+ \int_{T_-^h(\bar{w})}^{T_+^h(\bar{w})} \nabla H(\bar{\gamma}_0^h(t)) \cdot (G(0,0), -1)^T dt\bar{w} + \mathcal{O}(2). \end{aligned} \tag{A2}$$

Here $\mathcal{O}(2)$ denotes higher-order terms beyond quadratic in $\sqrt{\varepsilon}$ and $\bar{w}$. Considering the symmetry property, $(\bar{v}_0^h, \bar{z}_0^h)(-t) = (-\bar{v}_0^h, \bar{z}_0^h)(t)$ on $\bar{\gamma}_0^h$, we invoke the time-reversal transformation $t \mapsto -t$. Substituting this symmetry into the integral formulation yields $\int_{T_-^h(\bar{w})}^{T_+^h(\bar{w})} \frac{\partial H}{\partial \bar{v}}(\bar{\gamma}_0^h(t))F(0,0)dt = \int_{T_-^h(\bar{w})}^{T_+^h(\bar{w})} \frac{\partial H}{\partial \bar{v}}(\bar{\gamma}_0^h(t))G(0,0)dt = 0$. Consequently, we derive the first-order expansion $\hat{h} - h = \sqrt{\varepsilon}d_{\sqrt{\varepsilon}}^h + \bar{w}d_{\bar{w}}^h + \mathcal{O}(2)$, where the coefficients $d_{\sqrt{\varepsilon}}^h$ and $d_{\bar{w}}^h$ are explicitly defined in Refs. [2,25,33,34]. Furthermore, the asymptotic expression for $\bar{w}'$ in system Eq. (2.4b) satisfies

$$\bar{v} = -\frac{1}{2}(-\bar{z}' + 59.998\bar{w} - 0.002\sqrt{\varepsilon}\bar{z} + 81.00703), \tag{A3}$$

let $\chi = a - c - bz_0 + dw_0 - 2 = 81.00703$, then

$$\bar{v} = -\frac{1}{2}(-\bar{z}' + 59.998\bar{w} - 0.002\sqrt{\varepsilon}\bar{z} + \chi) = \frac{1}{2}(\bar{z}' - 59.998\bar{w} + 0.002\sqrt{\varepsilon}\bar{z} - \chi). \tag{A4}$$

To incorporate (A4) into (2.4c), we substitute it into the expression for (2.4c) as

$$\bar{w}' = \varepsilon(\mu - \sqrt{\varepsilon}(60\bar{w} + \frac{1}{2}(\bar{z}' - 59.998\bar{w} + 0.002\sqrt{\varepsilon}\bar{z} - \chi)), \tag{A5}$$

where $\mu = 1 + c - dw_0 = -83$, $\chi = a - c - bz_0 + dw_0 - 2 = 81.00703$ in Eq. (A5), leading to the simplified form in Eq. (A6). Similar to Eq. (A4) in Ref. [33], it implies

$$\begin{aligned} \bar{w}' &= \varepsilon(\mu - \sqrt{\varepsilon}(d\bar{w} + \frac{1}{2}(\bar{z}' - 59.998\bar{w} + 0.002\sqrt{\varepsilon}\bar{z} - \chi)) \\ &= (-\varepsilon\sqrt{\varepsilon}d + \frac{1}{2}\varepsilon\sqrt{\varepsilon}59.998)\bar{w} - \frac{1}{2}\varepsilon\sqrt{\varepsilon}(\bar{z}' + 0.002\sqrt{\varepsilon}\bar{z}) + \varepsilon(\mu - \frac{1}{2}\sqrt{\varepsilon}\chi) \\ &= -\frac{1}{2}\varepsilon\sqrt{\varepsilon}60.002\bar{w} - \frac{1}{2}\varepsilon\sqrt{\varepsilon}(\bar{z}' + 0.002\sqrt{\varepsilon}\bar{z}) + O(\varepsilon^2). \end{aligned} \tag{A6}$$

The general solution to the homogeneous counterpart of Eq. (A6) demonstrates an exponentially decaying behavior governed by the characteristic time scale $\frac{1}{\varepsilon\sqrt{\varepsilon}}$. This transient solution can be formulated as: $\bar{w}_h = Ce^{-\frac{1}{2}\varepsilon\sqrt{\varepsilon}60.002t}$, where C denotes the integration constant determined by initial conditions. After rigorous variation of constants method, we obtain the time-dependent coefficient characterizing the particular solution $C'(t) = -\frac{1}{2}\varepsilon\sqrt{\varepsilon}(\bar{z}' + 0.002\sqrt{\varepsilon}\bar{z})e^{\frac{1}{2}\varepsilon\sqrt{\varepsilon}60.002t}$. Therefore,

$$\begin{aligned}
C(t) =& -\frac{1}{60.002}(\bar{z}' + 0.002\sqrt{\varepsilon}\bar{z})e^{\frac{1}{2}\varepsilon\sqrt{\varepsilon}60.002t}\ |_{T_-^h(\bar{w})}^{t} \\
&+ \frac{1}{2}\varepsilon\sqrt{\varepsilon}\int_{T_-^h(\bar{w})}^{t} e^{\frac{1}{2}\varepsilon\sqrt{\varepsilon}60.002t}d(\bar{z}' + 0.002\sqrt{\varepsilon}\bar{z}), \\
=& -\frac{1}{60.002}(\bar{z}' + 0.002\sqrt{\varepsilon}\bar{z})e^{\frac{1}{2}\varepsilon\sqrt{\varepsilon}60.002t}\ |_{T_-^h(\bar{w})}^{t} \\
&+ \frac{1}{2}\varepsilon\sqrt{\varepsilon}\int_{T_-^h(\bar{w})}^{t} e^{\frac{1}{2}\varepsilon\sqrt{\varepsilon}60.002t}(\bar{z}''(s) + 0.002\sqrt{\varepsilon}\bar{z}'(s))ds, \\
=& -\frac{1}{60.002}(\bar{z}' + 0.002\sqrt{\varepsilon}\bar{z})(e^{\frac{1}{2}\varepsilon\sqrt{\varepsilon}60.002t} - e^{\frac{1}{2}\varepsilon\sqrt{\varepsilon}60.002T_-^h(\bar{w})}) \\
&+ \frac{1}{2}\varepsilon\sqrt{\varepsilon}\int_{T_-^h(\bar{w})}^{t} e^{\frac{1}{2}\varepsilon\sqrt{\varepsilon}60.002t}(\bar{z}''(s) + 0.002\sqrt{\varepsilon}\bar{z}'(s))ds.
\end{aligned} \tag{A7}$$

Furthermore, the solution of Eq. (A5) admits the analytical form

$$\begin{aligned}
\bar{w}(t) =& \bar{w}_h + C(t)e^{-30.001\varepsilon\sqrt{\varepsilon}t} = Ce^{-30.001\varepsilon\sqrt{\varepsilon}t} + C(t)e^{-\frac{1}{2}\varepsilon\sqrt{\varepsilon}60.002t} \\
=& Ce^{-30.001\varepsilon\sqrt{\varepsilon}t} - \frac{1}{60.002}(\bar{z}' + 0.002\sqrt{\varepsilon}\bar{z})(1 - e^{-30.001\varepsilon\sqrt{\varepsilon}(t-T_-^h(\bar{w}))}) \\
&+ \frac{1}{2}\varepsilon\sqrt{\varepsilon}\int_{T_-^h(\bar{w})}^{t} e^{30.001\varepsilon\sqrt{\varepsilon}t}(\bar{z}''(s) + 0.002\sqrt{\varepsilon}\bar{z}'(s))ds)\cdot e^{-30.001\varepsilon\sqrt{\varepsilon}t},
\end{aligned} \tag{A8}$$

where the corresponding homogeneous solution of Eq. (A5) takes the form of an exponentially attenuated profile $\bar{w}_h = Ce^{-30.001\varepsilon\sqrt{\varepsilon}t} = C(1 - 30.001\varepsilon\sqrt{\varepsilon}t + \mathcal{O}(\varepsilon^2t^2))$. Through variation of constants, the integration constant is determined by boundary matching $C = \bar{w}e^{30.001\varepsilon\sqrt{\varepsilon}T_-^h(\bar{w})}$. Substituting this into Eq. (A8) and evaluating at $t = T_+^h(\bar{w})$, we employ a first-order Taylor approximation for the exponential terms $e^{30.001\varepsilon\sqrt{\varepsilon}t} - e^{30.001\varepsilon\sqrt{\varepsilon}T_-^h(\bar{w})} = 30.001\varepsilon\sqrt{\varepsilon}(t - T_-^h(\bar{w}))$. Invoking the asymptotic identity $1 - e^{-x} \approx x$ for $x \ll 1$, and setting $t = T_+^h(\bar{w}))$, we ultimately derive

$$\begin{aligned}
\hat{\bar{w}} =& \bar{w}(1 - 30.001\varepsilon\sqrt{\varepsilon}T^h(\bar{w})) - \frac{\varepsilon\sqrt{\varepsilon}}{2}(\bar{z}' + 0.002\sqrt{\varepsilon}\bar{z})T^h(\bar{w}) \\
&+ \frac{1}{2}\varepsilon\sqrt{\varepsilon}\int_{T_-^h(\bar{w})}^{T_+^h(\bar{w})} e^{30.001\varepsilon\sqrt{\varepsilon}t}(\bar{z}''(t) + 0.002\sqrt{\varepsilon}\bar{z}'(t))dt\cdot e^{-30.001\varepsilon\sqrt{\varepsilon}T_+^h(\bar{w})} + \mathcal{O}(\varepsilon^2),
\end{aligned} \tag{A9}$$

recall that the temporal interval, $T^h(\bar{w}) = T_+^h(\bar{w}) - T_-^h(\bar{w})$ satisfies $T^h(\bar{w}) = \mathcal{O}(\sqrt{\varepsilon})$ in the $\bar{\Delta}_-$ regime [2, 25, 33, 34].

Crucially, while previous studies in Ref. [33] systematically omit the higher-order nonlinear term $2k\varepsilon\sqrt{\varepsilon}\bar{w}T^h(\bar{w})$ through scaling arguments, our analysis retains and rigorously accounts for the dominant singular perturbation term $\frac{1}{2}\varepsilon\sqrt{\varepsilon}(d+b)T^h(\bar{w})$ in Eq. (A9). This retention proves

essential for capturing the three-scale relaxation dynamics. Following asymptotic estimation of the remaining terms using the method of dominant balance, we obtain that

$$\begin{aligned}
&\int_{T_-^h(\bar{w})}^{T_+^h(\bar{w})} e^{30.001\varepsilon\sqrt{\varepsilon}t}(\bar{z}''(t)+0.002\sqrt{\varepsilon}\bar{z}'(t))dt\cdot e^{-30.001\varepsilon\sqrt{\varepsilon}T_+^h(\bar{w})}\\
=&\int_{T_-^h(\bar{w})}^{T_+^h(\bar{w})} e^{30.001\varepsilon\sqrt{\varepsilon}t}\bar{z}''(t)dt\cdot e^{-30.001\varepsilon\sqrt{\varepsilon}T_+^h(\bar{w})}\\
&+b\sqrt{\varepsilon}\int_{T_-^h(\bar{w})}^{T_+^h(\bar{w})} e^{30.001\varepsilon\sqrt{\varepsilon}t}\bar{z}'(t)dt\cdot e^{-\frac{1}{2}\varepsilon\sqrt{\varepsilon}(d+b)T_+^h(\bar{w})}\\
=&\mid f_1+f_2+f_3+f_4\mid\leq f_1+f_2+\mid f_3\mid+\mid f_4\mid. \qquad \text{(A10)}
\end{aligned}$$

Under the scaling condition $\bar{z}=\mathcal{O}(1)$, our asymptotic analysis reveals that the nonlinear components f_2 and f_4, when multiplied by their respective exponential factors, remain bounded throughout the temporal domain. Crucially, these terms contribute only higher-order corrections to the dynamics $f_2, f_4 = \mathcal{O}(\varepsilon^{\frac{3}{2}})$. In contrast, the dominant contributions emerge from f_1 and f_3, whose structures are prescribed by boundary layer matching [2, 25, 33, 34]: $f_1=0.002\sqrt{\varepsilon}(\bar{z}(T_+^h(\bar{w}))-\bar{z}(T_-^h(\bar{w}))+\mathcal{O}(\varepsilon^2 T_\pm^h(\bar{w}))$, and $f_3=\bar{z}'(T_+^h(\bar{w}))-\bar{z}'(T_-^h(\bar{w}))+\mathcal{O}(\varepsilon^2 T_\pm^h(\bar{w}))$. Given the slow variable scaling $\bar{z}=\mathcal{O}(1), \bar{z}'=\mathcal{O}(1)$, we establish the critical scaling relationships $\bar{z}(T_+^h(\bar{w})-\bar{z}(T_-^h(\bar{w})=\mathcal{O}(\varepsilon^2)$ and $\bar{z}'(T_+^h(\bar{w})-\bar{z}'(T_-^h(\bar{w})=\mathcal{O}(\varepsilon^2)$. Within the $\bar{\Delta}_-$ regime, these scaling laws induce corresponding higher-order perturbations in the Hamiltonian structure $H(0,\bar{z}(T_+^h(\bar{w}))-H(0,\bar{z}(T_-^h(\bar{w}))=\mathcal{O}(\varepsilon^2)$, as rigorously demonstrated in prior multiscale analyses [2, 25, 33, 34].

$$\begin{aligned}
\hat{\bar{w}}=&\bar{w}(1-30.001\varepsilon\sqrt{\varepsilon}T^h(\bar{w}))-\frac{\varepsilon\sqrt{\varepsilon}}{2}(\bar{z}'+0.002\sqrt{\varepsilon}\bar{z})T^h(\bar{w})\\
&+\frac{1}{2}\varepsilon\sqrt{\varepsilon}(f_1+f_2+f_3+f_4)+\mathcal{O}(\varepsilon^2)\leq\bar{w}(1-30.001\varepsilon\sqrt{\varepsilon}T^h(\bar{w}))\\
&-\frac{\varepsilon\sqrt{\varepsilon}}{2}(c_1+0.002\sqrt{\varepsilon}c_2)T^h(\bar{w})+\frac{1}{2}\varepsilon\sqrt{\varepsilon}(0.002\sqrt{\varepsilon}c_3\\
&+c_4+0.030001\varepsilon^2c_5+30.001\varepsilon\sqrt{\varepsilon}c_6)+\mathcal{O}(\varepsilon^2). \qquad \text{(A11)}
\end{aligned}$$

We therefore establish the asymptotic solution $\hat{\bar{w}}=\bar{w}(1-30.001\varepsilon\sqrt{\varepsilon}T^h(\bar{w}))+\mathcal{O}(\varepsilon^2)$. The complete mathematical justification for Eq. (3.1), including the derivative operators $d^h_{\sqrt{\varepsilon}}$ and $d^h_{\bar{w}}$, is rigorously developed in Lemmas A.3∼A.5 of Ref. [20]. Building upon this theoretical foundation, we extend the analysis to initial conditions admitting the parameterization: $\bar{w}'=\varepsilon(\mu-g_1\varepsilon\bar{z})$. Through systematic integration of Eq. (2.4c) and substitution of the slow variable decomposition $\bar{z}=-\bar{v}'+\bar{v}^2-\frac{1}{3}\sqrt{\varepsilon}\bar{v}^3$, we derive the leading-order asymptotic mapping $\hat{w}\sim\bar{w}+\varepsilon(2\mu T^h-g_1\varepsilon\int_{-T^h}^{T^h}(-\bar{v}'(t)+\bar{v}^2(t)-\frac{1}{3}\sqrt{\varepsilon}\bar{v}^3(t))dt$ [2, 25, 33, 34]. This result fundamentally characterizes the parametric dependence of the transition layer dynamics. Subsequent analysis focuses on verifying solution consistency within the parameter regime, particularly examining the stability criteria for $\bar{w}$-dependent equilibria. □

B. Appendix 2

Proof of Proposition 3.2. Guided by the scaling law $w^{\text{in}}=\mathcal{O}(\varepsilon)$ stipulated in Assumption 3.1, we derive the proof of asymptotic boundedness firstly. Let $\varepsilon_0>0$ be the characteristic

scaling parameter, there exists $C > 0$ such that $\sup_{\varepsilon\in(0,\varepsilon_0)} \left\| \frac{w^{\text{in}}}{\sqrt{\varepsilon}} \right\|_{L^\infty} \leq C$. This uniform bound (Proposition 3.2) ensures well-posedness of the boundary layer approximation when $\varepsilon \to 0$. Therefore, we change Eqs. (2.4) into [2,25,33,34]

$$\begin{cases} \bar{v}' = \bar{z} + \bar{v}^2 - \dfrac{1}{3}\sqrt{\varepsilon}\bar{v}^3, & \text{(A1a)} \\ \bar{z}' = \dfrac{-1}{\sqrt{\varepsilon}}(\sqrt{\varepsilon}\bar{v} - 1.99237 - 0.002(-\varepsilon\bar{z} + \sqrt{\varepsilon}w + 0.3)), & \text{(A1b)} \\ \bar{w}' = \varepsilon(\mu + \phi(v, z, w)) = \varepsilon(\mu - g_1 z), & \text{(A1c)} \end{cases}$$

here the parametric scaling is defined as $\mu = -\frac{83}{\sqrt{\varepsilon}}$ with the auxiliary function $\phi(v, z, w) = -\bar{v} - 60\bar{w} = -\varepsilon g_1 z$. The algebraic constraint in Eqs. (2.2a)-(2.2c) induces the functional relationship $z + v^2 - \frac{1}{3}v^3 = 0 \Rightarrow z = f(v) = -v^2 + \frac{1}{3}v^3$. Differentiating this constraint yields the differential compatibility condition $z' = f'(v)v' = (-2v + v^2)v'$. Through these transformations, the original system (2.2a)-(2.2c) reduces to the canonical singular perturbation form

$$\begin{cases} f'(v)v' = \varepsilon(-1)(v - 1.99237 - 0.002(-z + w + 0.3)), & \text{(A2a)} \\ w' = \varepsilon^2(-v - 29 - 60(w + 0.9)). & \text{(A2b)} \end{cases}$$

Consequently, we obtain the desingularized form of (A2a)-(A2b)

$$\begin{cases} v' = \varepsilon(v - 1.99237 - 0.002(-z + w + 0.3)), & \text{(A3a)} \\ w' = \varepsilon^2(-v - 29 - 60(w + 0.9))(2v - v^2). & \text{(A3b)} \end{cases}$$

However, through systematic manipulation of the governing Eqs. (A2a)-(A2b), we establish the characteristic relationship $w' = \varepsilon(\mu - g_1 z) = \varepsilon(\mu - g_1 f(v))$ where the coefficients are explicitly determined as $\mu = -29 - 60(w + 0.9), g_1 = 1$. By introducing the composite state variable $W = \frac{w}{v}$, we obtain the desingularized dynamical system

$$\begin{cases} v' = -v(1 - w), & \text{(A4a)} \\ W' = W(1 - W) - \varepsilon(\mu - g_1(-v^2 + \dfrac{1}{3}v^3))(2v - v^2), & \text{(A4b)} \end{cases}$$

utilizing the Neumann series expansion for operator inversion $(1-W)^{-1} = 1+W+\mathcal{O}(W^2)$ where the convergence radius condition $\|W\| < 1$ is explicitly specified [2,25,33,34], Eqs. (A4a)-(A4b) becomes

$$\begin{cases} \dfrac{dv}{d\tilde{t}} = -v, & \text{(A5a)} \\ \dfrac{dW}{d\tilde{t}} = (1 - 2\mu\varepsilon)W - 2\mu\varepsilon + \mu\varepsilon v, & \text{(A5b)} \end{cases}$$

here this transformation $\tilde{t}$ introduces the rescaled time variable.

Implementing the method of matched asymptotic expansions, we prescribe inner layer $v = -\rho$ in Σ^{in} and transition layer $v = -\alpha\sqrt{\varepsilon}$, in Δ^{in}. The transition time $\tilde{T}$ between (A5a)-(A5b) (visualized in Figures 1(e) and (f)) is determined by solving the leading-order system (A4a)-(A4b), giving that $\tilde{T}$ satisfies $e^{\tilde{T}} = \frac{\rho}{\alpha}\frac{1}{\sqrt{\varepsilon}}$. Substituting $\varepsilon v(\tilde{T}) = -\varepsilon\rho e^{-\tilde{T}} = \mathcal{O}(\varepsilon^2)$ into Eq. (A5b) produces the corrected solution $W(\tilde{T}) = (W^{\text{in}} - 2\mu\varepsilon)e^{(1-2\mu\varepsilon)\tilde{T}} - 2\mu\varepsilon + \mu\varepsilon v + \mathcal{O}(\varepsilon^2)$, where $W^{\text{in}} = -\frac{w^{\text{in}}}{\rho}$. The scaling $w = \alpha\sqrt{\varepsilon}W(\tilde{T})$ maintains consistency across all asymptotic regions.

Through asymptotic expansion of the w-parameter we derive the time-dependent solution $w(T) = w^{\text{in}} + w^{\text{in}}\mu\varepsilon\ln\varepsilon + \mathcal{O}(\varepsilon)$, where $T \in \mathbb{R}^+$(transition time). Given the scaling relationship $\bar{w} = \frac{w}{\sqrt{\varepsilon}}$, substitution yields $\bar{w} = \frac{w(T)}{\sqrt{\varepsilon}} = \frac{w^{\text{in}}}{\sqrt{\varepsilon}} + w^{\text{in}}\mu\sqrt{\varepsilon}\ln\varepsilon + \mathrm{O}(\sqrt{\varepsilon})$. The construction of h^- exploits the near-integrable structure of Eqs. (2.4a)-(2.4c). Specifically, the trajectory in $(\bar{v}, \bar{z}, \bar{w})$-space admits the asymptotic expansion: $h^- = \sqrt{\varepsilon}d^-_{\sqrt{\varepsilon}} + \bar{w}d^-_{\bar{w}} + O(2)$, where the integration bounds $d^-_{\sqrt{\varepsilon}}$ and $d^-_{\bar{w}}$ correspond to the singular limit $T^h_+(0) \to \infty$ as $h \to 0$ [2,25,33,34]. The singular set $C^-_\varepsilon \subset \bar{\Delta}_-$ is defined as the set comprising terminal points of trajectories originating from S^{a-}_ε. Through the scaling transformation $\bar{w} = \frac{w}{\sqrt{\varepsilon}}$, we establish its asymptotic characterization $h^-(\bar{w}, \sqrt{\varepsilon}) = \sqrt{\varepsilon}d^-_{\sqrt{\varepsilon}} + \frac{w^{\text{in}}}{\sqrt{\varepsilon}}d^-_{\bar{w}} + O(2)$. The leading-order dynamics on S^r_ε are governed by Melnikov-type integrals $d^+_{\sqrt{\varepsilon}} = -\int_0^\infty \nabla H(\bar{\gamma}^0_0(t)) \cdot (-\frac{1}{3}\bar{v}^0_0(t)^3, 0)^T dt$ and $d^+_{\bar{w}} = -\int_0^\infty \nabla H(\bar{\gamma}^0_0(t)) \cdot (0, -1)^T dt$. The conjugate singular set C^+_ε admits analogous parameterization $h^+(\bar{w}, \sqrt{\varepsilon}) = \sqrt{\varepsilon}d^+_{\sqrt{\varepsilon}} + \frac{w^{\text{in}}}{\sqrt{\varepsilon}}d^+_{\bar{w}} + O(2)$, with coefficients satisfying the symmetry relations $d^\pm_{\sqrt{\varepsilon}} = \mp\frac{1}{2}d^0_{\sqrt{\varepsilon}}$ and $d^\pm_{\bar{w}} = \mp\frac{1}{2}d^0_{\bar{w}}$ which are depicted as below [2,25,33,34]. □

C. Appendix 3

Proof of Proposition 3.3. Consider the parameter regime $(h, \bar{w}) \in \bar{\Delta}_-$ with $h < 0$, satisfying the asymptotic condition $h = O(\varepsilon^M)$ for some $M > 0$. The transition time $T^{h,out}(\bar{w})$, governed by the outer map Π^{out}, quantifies the phase space transport between $\bar{\Delta}_-$ and $\bar{\Delta}^{\text{out}}$. By applying Proposition 3.1, we rigorously obtain the quasi-integrable system (2.4a)-(2.4c)

$$\begin{aligned}\bar{\Pi}^{\text{out}}(h, \bar{w}) &= (h^{\text{out}}, \bar{w}^{\text{out}}) \\ &= (h + \sqrt{\varepsilon}d^{\text{out}}_{\sqrt{\varepsilon}} + \bar{w}d^{\text{out}}_{\bar{w}} + O(2), \\ &\quad \bar{w} + (-\varepsilon)(b\varepsilon^{\frac{3}{2}}\bar{z} + \bar{z}' - 0.002\sqrt{\varepsilon}z_0)(T^{h,\text{out}}(\bar{w}) + O(\varepsilon^2)),\end{aligned} \tag{A1}$$

where the asymptotic coefficients $d^{\text{out}}_{\sqrt{\varepsilon}}$ and $d^{\text{out}}_{\bar{w}}$ are defined as above; see also the proof of Proposition 3.1. Specifically, these quantities satisfy the geometric constraint relations: Where the differentiation procedure follows the standard Gâteaux derivative formalism in GSPT [2,25, 33,34]. Complete technical details of their construction are provided in the proof of Proposition 3.1.

To characterize the second map transition from $\bar{\Delta}^{\text{out}}$ to Σ^{out} in Eqs. (2.2a)-(2.2c), we introduce the coordinate transformation $z = v^2 Z$ near the origin. This scaling is followed by factorization of $\Phi(v, Z)$ as: $\Phi(v, Z) = v^2(-Z + 1 - \frac{1}{3}v)$

$$\begin{cases} \dfrac{dv}{d\hat{t}} = 1, & \text{(A2a)} \\ \dfrac{dZ}{d\hat{t}} = -\dfrac{2}{v}Z + \dfrac{\varepsilon(-1)(v - 1.99237 - 0.002(-v^2Z + w + Z_0))}{v^2\Phi(v, Z)}, & \text{(A2b)} \\ \dfrac{dw}{d\hat{t}} = \dfrac{\varepsilon^2}{\Phi(v, Z)}(-v - 29 - 60(w + 0.9)), & \text{(A2c)} \end{cases}$$

here, $\hat{t}$ denotes the transformed temporal coordinate. Notably, Δ^{out} corresponds to the projection of $\bar{\Delta}^{\text{out}}$ onto the (v, Z, w)-plane.

Given an initial condition v^{out} for the system governed by Eqs. (2.2a)-(2.2c) in $\bar{\Delta}^{\text{out}}$, the scaling relationship $v^{\text{out}} = O(\sqrt{\varepsilon}T^{h,out}(\bar{w})) = O(\sqrt{-\varepsilon\ln\varepsilon})$ emerges. Consequently, we deduce

that $w = O(\varepsilon)$, where maintains a diminutive magnitude throughout the process. Specifically, from Eq. (A2c), the derivative $\frac{dw}{d\hat{t}} = O(\varepsilon(\ln\varepsilon)^{-1})$ suggests that w remains quasi $\Phi(v, Z)$ in Eq. (A2c) yields

$$\begin{cases} \dfrac{dv}{d\hat{t}} = 1, & \text{(A3a)} \\ \dfrac{dZ}{d\hat{t}} = -\dfrac{2}{v}Z + \dfrac{\varepsilon}{-v^3}(1 + O(v, Z, w)). & \text{(A3b)} \end{cases}$$

As shown in Figure 1(e) and (f), the geometric mapping from Δ^{out} to Σ^{out} under the governing Eqs. (A3a)-(A3b) is explicitly demonstrated. For $(v^{\text{out}}, Z^{\text{out}}) \in \Delta^{\text{out}}$, the analytical solution of Eqs. (A3a)-(A3b) can be expressed as: $Z(v) = \frac{(v^{\text{out}})^2 Z^{\text{out}}}{v^2} + \frac{\varepsilon}{-v^2}\ln\frac{\text{v}}{\text{v}^{\text{out}}} + \text{O}(\varepsilon)$. Notably, higher-order terms $O(v, Z, w)$ in Eqs. (A3a)-(A3b) have been systematically neglected during the derivation process. This simplification yields the reduced form: $z(v) = \varepsilon\tilde{z}^{\text{out}} + \frac{\varepsilon}{-v^2}\ln\frac{\text{v}}{\text{v}^{\text{out}}} + \text{O}(\varepsilon)$ where $\tilde{z}^{\text{out}}$ in $\bar{\Delta}^{\text{out}}$ and $z = v^2 Z = \varepsilon\tilde{z}$. Considering the asymptotic behavior $v^{\text{out}} = O(\sqrt{-\varepsilon\ln\varepsilon})$ and $v = \delta$ in Σ^{out}, the temporal evolution during the transition phase can be characterized as: $z(T) = \varepsilon\tilde{z}^{\text{out}} + O(\varepsilon\ln\varepsilon)$. Here, T denotes the characteristic transition time scale [2, 25, 33, 34].

Due to $dv = \Phi(v, Z)dt$ and $Z = o(1)$, we derive the inequality $\frac{1}{2}\Phi(v, 0) \leq \Phi(v, Z)$, which implies the time $T \leq 2\int_{v^{\text{out}}}^{\delta} \frac{dv}{\Phi(v,0)}$. Furthermore, through asymptotic analysis, we obtain $T \leq \frac{2}{v^{\text{out}}} + \frac{1}{3}\ln\varepsilon + \text{O}(1)$. Moreover, w is expressed as $w' = \varepsilon^2(-v - 29 - 60(w + 0.9)) = \varepsilon^2(-v - 60w - 83)$, where the nonlinear term originates from the coupling with Eq. (A1). Integrating this equation while considering the functional form $\psi(v, Z) = v^2(Z + 1 - \frac{1}{3}v)$, we evaluate the baseline case $\psi(v, 0) = v^2(1 - \frac{1}{3}v)$. This yields $w(T) = \sqrt{\varepsilon}\bar{w}^{\text{out}} + \varepsilon^2((1 + c - dw_0)T - \sqrt{\varepsilon}d\bar{w}^{\text{out}}T - \int_{v^{\text{out}}}^{\delta} \frac{v}{v^2(1-\frac{1}{3}v)}dv) + O(\varepsilon^3)$. Therefore, there exists $\int \frac{v}{v^2(1-\frac{1}{3}v)}dv = \int \frac{1}{v(1-\frac{1}{3}v)}dv = \ln\frac{\text{v}}{3-\text{v}} - 30$, thus substituting back and applying the perturbation scaling $w = \sqrt{\varepsilon}\bar{w}$, we conclude $w(T) = \sqrt{\varepsilon}\bar{w} - 83\varepsilon\sqrt{\varepsilon}T^{h,out}(\bar{w}) + O(\varepsilon\sqrt{\varepsilon})$, where the system parameter $k = \frac{83}{60}$ characterizes the nonlinear coupling strength under the perturbation constraint $0 < \varepsilon \ll 1$. □

References

[1] L. Arnold, C. Jones, K. Mischaikow, G. Raugel and C. Jones, *Geometric Singular Perturbation Theory*, volume 44–118, Springer, Brown University, 1995.

[2] K. R. T. J. Christopher and I. K. Alexander, *Multiple-Time-Scale Dynamical Systems*, volume 122, Springer, Springer-Verlag New York, 2001.

[3] R. Curtu and J. Rubin, *Interaction of canard and singular Hopf mechanisms in a neural model*, SIAM J. Appl. Dyn. Syst., 2011, 10(4), 1443–1479.

[4] M. Desroches, J. Guckenheimer, B. Krauskopf, C. Kuehn, H. M. Osinga and M. Wechselberger, *Mixed-mode oscillations with multiple time scales*, SIAM Review, 2012, 54(2), 211–288.

[5] S. Dong, H. Su, R. Hou and A. Shankar, *Improved pbft consensus mechanism based on voting sort clustering partition with group signature for IoT*, IEEE Transactions on Intelligent Transportation Systems, 2024, 26(2), 2239–2251.

[6] S. Dong, H. Su, Y. Xia, F. Zhu, X. Hu and B. Wang, *A comprehensive survey on authentication and attack detection schemes that threaten it in vehicular ad-hoc networks*, IEEE Transactions on Intelligent Transportation Systems, 2023, 24(12), 13573–13602.

[7] S. Dong, Y. Xia and J. Kamruzzaman, *Quantum particle swarm optimization for task offloading in mobile edge computing*, IEEE Transactions on Industrial Informatics, 2022, 19(8), 9113–9122.

[8] F. Dumortier, *Techniques in the theory of local bifurcations: Blow-up, normal forms, nilpotent bifurcations, singular perturbations*, Bifurcations and Periodic Orbits of Vector Fields, 1993, 19–73.

[9] Y. Endo and K. Takeda, *Performance evaluation of matrix factorization for fMRI data*, Neural Comput., 2023, 36(1), 128–150.

[10] J. Fan, G.-A. Yu, M. Zhao and H. Zong, *Addressing multi-scale temporal variability: Deep integration and application of the cnn and transformer model in monthly streamflow prediction*, Expert Systems with Applications, 2025, 292, 128658.

[11] J. Fan, G.-A. Yu, M. Zhao and H. Zong, *MCPT-CAF-BiGRU: A multi-scale CNN and ProbSparse-Masked Transformer model with cross-attention fusion and BiGRU for hourly wind speed forecasting*, Expert Systems with Applications, 2026, 307, 131081.

[12] R. FitzHugh, *Impulses and physiological states in theoretical models of nerve membrane*, Biophys. J., 1961, 1(6), 445–466.

[13] I. Ghosh, H. O. Fatoyinbo and S. S. Muni, *Comprehensive analysis of slow-fast denatured morris-lecar neurons*, Phys. Rev. E, 2025, 111(4), 044204.

[14] J. Guckenheimer, *Singular Hopf bifurcation in systems with two slow variables*, SIAM J. Appl. Dyn. Syst., 2008, 7(4), 1355–1377.

[15] J. Guckenheimer and C. Scheper, *A geometric model for mixed-mode oscillations in a chemical system*, SIAM J. Appl. Dyn. Syst., 2011, 10(1), 92–128.

[16] J. Guckenheimer and A. R. Willms, *Asymptotic analysis of subcritical Hopf–homoclinic bifurcation*, Physica D, 2000, 139(3–4), 195–216.

[17] A. L. Hodgkin and A. F. Huxley, *A quantitative description of membrane current and its application to conduction and excitation in nerve*, J. Physiol., 1952, 117(4), 500.

[18] E. M. Izhikevich, *Dynamical Systems in Neuroscience*, volume 1, MIT Press, Cambridge, Massachusetts London, England, 2006.

[19] M. T. M. Koper, *Bifurcations of mixed-mode oscillations in a three-variable autonomous Van der Pol-Duffing model with a cross-shaped phase diagram*, Phys. D., 1995, 80(1), 72–94.

[20] M. Krupa, N. Popović and N. Kopell, *Mixed-mode oscillations in three time-scale systems: A prototypical example*, SIAM J. Appl. Dyn. Syst., 2008, 7(2), 361–420.

[21] M. Krupa, N. Popović, N. Kopell and H. G. Rotstein, *Mixed-mode oscillations in a three time-scale model for the dopaminergic neuron*, Chaos, 2008, 18(1), 015106.

[22] M. Krupa and P. Szmolyan, *Extending geometric singular perturbation theory to nonhyperbolic points—fold and canard points in two dimensions*, SIAM J. Math. Anal., 2001, 33(2), 286–314.

[23] M. Krupa and P. Szmolyan, *Relaxation oscillation and canard explosion*, J. Differ. Equ., 2001, 174(2), 312–368.

[24] M. Krupa and M. Wechselberger, *Local analysis near a folded saddle-node singularity*, J. Differ. Equ., 2010, 248(12), 2841–2888.

[25] C. Kuehn, *Multiple Time Scale Dynamics*, volume 191, Springer, Cham Heidelberg New York Dordrecht London, 2015.

[26] X. Lin, Y. Liu and S. Liu, *Torus bifurcation and homoclinic chaos underlie potassium-driven epileptiform dynamics in a multi-timescale neural mass model*, Chaos Solition. Fract., 2026, 208, 118204.

[27] W. Liu, X. Que and Y. Wang, *H_∞ control observer-based for discrete-time singularly perturbed systems with nonlinear disturbances*, IEEE Access, 2022, 10, 14496–14506.

[28] W. Liu and Y. Wang, *Passivity-based sliding mode control for lur'e singularly perturbed time-delay systems with input nonlinearity*, Circuits, Systems, and Signal Processing, 2022, 41(11), 6007–6030.

[29] W. Liu, Y. Wang and Y. Tian, *Feedback stabilization for discrete-time singularly perturbed systems via limited information with data packet dropout*, IEEE Access, 2021, 9, 40585–40594.

[30] W. Liu, Y. Wang and Z. Wang, *Robust input-to-state stability of discrete-time singularly perturbed systems with nonlinear perturbation*, Nonlinear Dynamics, 2022, 109(4), 2935–2948.

[31] Y. Liu, Y. Xia and J. Kurths, *Emergence of shilnikov homoclinic bifurcation and orbit-induced mixed-mode oscillations in a neuronal dynamical system*, Chaos Solition. Fract., 2025, 200, 116893.

[32] J. Ma and J. Tang, *A review for dynamics of collective behaviors of network of neurons*, Sci. China Technol. Sci., 2015, 58, 2038–2045.

[33] D. P. Maesschalck, E. Kutafina and N. Popović, *Three time-scales in an extended Bonhoeffer–van der Pol oscillator*, J. Dyn. Differ. Equ., 2014, 26, 955–987.

[34] D. P. Maesschalck, E. Kutafina and N. Popović, *Three Time-Scales in an Extended Bonhoeffer-Van der Pol Oscillator*, volume 1, Edinburgh Research Explorer, The University of Edinburgh, 2014.

[35] C. Magnani and L. E. Moore, *Power spectral analysis of voltage-gated channels in neurons*, Front. Neuroinf., 2025, 18, 1472499.

[36] M. Martin and M. G. Pedersen, *Modelling and analysis of cAMP-induced mixed-mode oscillations in cortical neurons: Critical roles of HCN and M-type potassium channels*, PLoS Comput. Biol., 2024, 20(3), e1011559.

[37] A. Mondal, A. Mondal, S. K. Sharma, R. K. Upadhyay and C. G. Antonopoulos, *Spatiotemporal characteristics in systems of diffusively coupled excitable slow–fast FitzHugh–Rinzel dynamical neurons*, Chaos, 2021, 31(10), 103122.

[38] J. Nagumo, S. Arimoto and S. Yoshizawa, *An active pulse transmission line simulating nerve axon*, Proc. IRE, 1962, 50(10), 2061–2070.

[39] Y. Patsios, R. Huzak, P. De Maesschalck and N. Popović, *Jump-induced mixed-mode oscillations through piecewise-affine maps*, J. Math. Anal. Appl., 2022, 505(1), 125641.

[40] J. Rinzel, *Repetitive activity and Hopf bifurcation under point-stimulation for a simple FitzHugh-Nagumo nerve conduction model*, J. Math. Biol., 1977, 5, 363–382.

[41] A. Roberts, *Canard explosion and relaxation oscillation in planar, piecewise-smooth, continuous systems*, SIAM J. Appl. Dyn. Syst., 2016, 15(1), 609–624.

[42] H. G. Rotstein, *Mixed-Mode Oscillations in Single Neurons*, in Encyclopedia of Computational Neuroscience, Springer, 2022, 2046–2053.

[43] H. G. Rotstein, M. Wechselberger and N. Kopell, *Canard induced mixed-mode oscillations in a medial entorhinal cortex layer ii stellate cell model*, SIAM J. Appl. Dyn. Syst., 2008, 7(4), 1582–1611.

[44] J. Rubin and M. Wechselberger, *Giant squid-hidden canard: The 3D geometry of the Hodgkin–Huxley model*, Biol. Cybern., 2007, 97, 5–32.

[45] C. Scheper, *Multiple Time Scale Dynamics Of Chemical Oscillators*, volume 1, eCommons, Cornell University, 2011.

[46] D. Senkowski and A. K. Engel, *Multi-timescale neural dynamics for multisensory integration*, Nat. Rev. Neurosci, 2024, 25(9), 625–642.

[47] S. K. Sharma, A. Mondal, A. Mondal, M. A. Aziz-Alaoui, R. K. Upadhyay and J. Ma, *Emergence of canard induced mixed mode oscillations in a slow–fast dynamics of a biophysical excitable model*, Chaos Solition. Fract., 2022, 164, 112669.

[48] B. Song and Y. Liu, *Review on mixed-mode oscillations dynamics based on neuron models and neural networks*, Eur. Phys. J. Spec. Top., 2026, 234(9), 8759–8778.

[49] W. Sun, Q. G. Yin, H. H. Wan, R. R. Gao, C. Xiong, C. Xie, X. X. Meng, Y. L. Mi, X. T. Wang, C. X. Wang, et al., *Characterization of the horse chestnut genome reveals the evolution of aescin and aesculin biosynthesis*, Nat. Commun., 2023, 14(1), 6470.

[50] Y. Sun and J. Zhao, *Regional passivity for switched nonlinear systems and its application*, ISA Transactions, 2019, 86, 98–109.

[51] Y. Wang, W. Liu, G. Liu and Y. Zhai, *Robust dynamic output feedback control for uncertain fast sampling discrete-time singularly perturbed systems*, Circuits, Systems, and Signal Processing, 2020, 39(7), 3372–3388.

[52] M. Wechselberger, *Existence and bifurcation of canards in R^3 in the case of a folded node*, SIAM J. Appl. Dyn. Syst., 2005, 4(1), 101–139.

[53] W. X. Xie, J. W. Xu, L. Cai and Y. F. Jin, *Dynamics and geometric desingularization of the multiple time scale FitzHugh Nagumo Rinzel model with fold singularity*, Commun. Nonlinear. Sci. Numer. Simul., 2018, 63, 322–338.

[54] A. M. Zhabotinskii, *Periodic kinetics of oxidation of malonic acid in solution (study of the Belousov reaction kinetics)*, Biofizika, 1964, 9(1), 306–311.

[55] R. L. Zhang, Z. Y. Wang, T. Y. Wu, Y. H. Cai, L. Tao, Z. C. Xiao and Y. Li, *Learning spiking neuronal networks with artificial neural networks: Neural oscillations*, J. Math. Biol., 2024, 88(6), 65.

[56] S. Zhu, X. Tian, Z. Zhang, R. Qiao and H. Zhu, *Content placement and edge collaborative caching scheme based on deep reinforcement learning for internet of vehicles*, IEEE Transactions on Intelligent Transportation Systems, 2025.

Received May 2025; Accepted October 2026; Available online November 2026.